Cell Reports, Volume *22*

Supplemental Information

Aspirin Recapitulates Features of Caloric Restriction

Federico Pietrocola, Francesca Castoldi, Maria Markaki, Sylvie Lachkar, Guo Chen, David P. Enot, Sylvere Durand, Noelie Bossut, Mingming Tong, Shoaib A. Malik, Friedemann Loos, Nicolas Dupont, Guillermo Mariño, Nejma Abdelkader, Frank Madeo, Maria Chiara Maiuri, Romano Kroemer, Patrice Codogno, Junichi Sadoshima, Nektarios Tavernarakis, and Guido Kroemer

Supporting informations

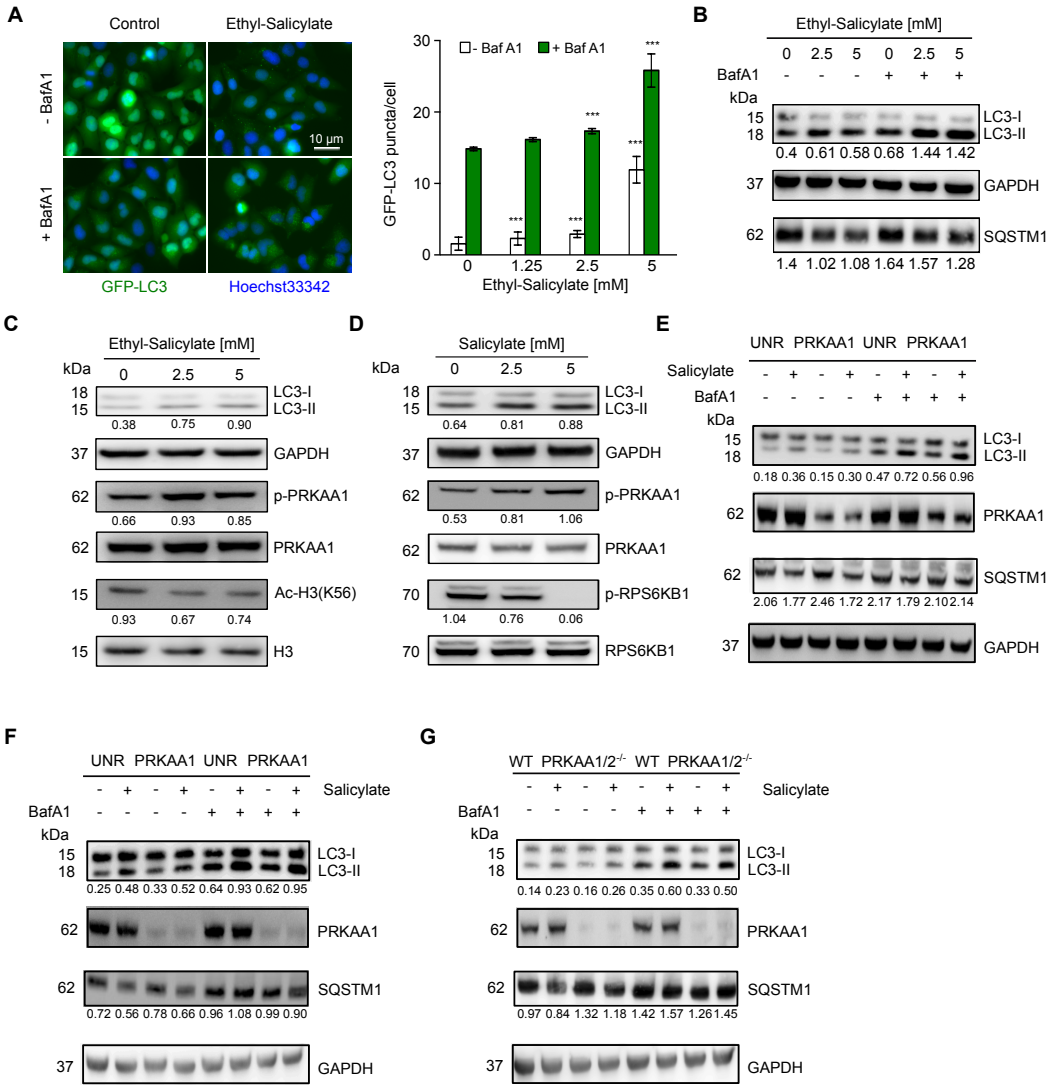

Supplemental Figure 1 (related to Figure 2 and 3). Ethyl-Salicylate induces autophagic flux and inhibits EP300. (**A**) U2OS cells expressing green fluorescent protein (GFP)-LC3 were treated with ethyl-salicylate for 8 h. Addition of Bafilomycin A1 allowed measuring autophagic flux. Representative images (left panel) and quantification (right panel) are shown. Data represent means ± SD from one representative experiment. *** $p < 0.001$; (unpaired t test, as compared with control condition). (**B,C**) HCT116 human colorectal cells were incubated for 8 hours in presence of growing concentrations of ethyl-salicylate. (**B**) Representative immunoblots of three independent experiments showing LC3I to LC3II conversion (in presence or absence of BafA1), (**C**) reduction in the acetylation levels of the EP300 substrate H3K56, (**B**) depletion of the autophagic substrate SQSTM1 and **(C)** activation of PRKAA, as monitored by Thr172 phosphorylation. (**D**) Salicylate modulates nutrient-sensing signaling pathways. Treatment of HCT116 with salicylate promotes the activation of

autophagy (as monitored by LC3-I to LC3-II conversion) along with the activation of PRKAA and the inhibition of mTORC1 signaling (as monitored by a decrease in Thr389 phosphorylation of p70 S6 Kinase [PRS6K1]). (**E**) Salicylate-induced autophagy does not require PRKAA activation. HCT116 cells were transfected with an unrelated (UNR) or with a small interfering RNA (siRNA) targeting PRKAA α1 subunit, followed by treatment with of salicylate for 16 hours. Representative immunoblots of three independent experiments showing the increased LC3I to LC3II conversion (in presence or absence of BafA1), the autophagy-dependent degradation of SQSTM1/p62 and the effective silencing of PRKAA1. (**F)** U2OS cells were transfected with an unrelated (UNR) or with a small interfering RNA (siRNA) sequence targeting PRKAA1 subunit and treated with salicylate. Autophagy and effective PRKAA silencing were monitored as previously described. (**G**) Mouse Embryonic Fibroblasts (MEF) Wild Type (WT) or their PRKAA deficient counterparts (PRKAA1/2$^{-/-}$) were treated for 16 hours with 5 mM salicylate and autophagy was monitored by immunoblotting in presence or absence of BafA1 to measure autophagic flux.

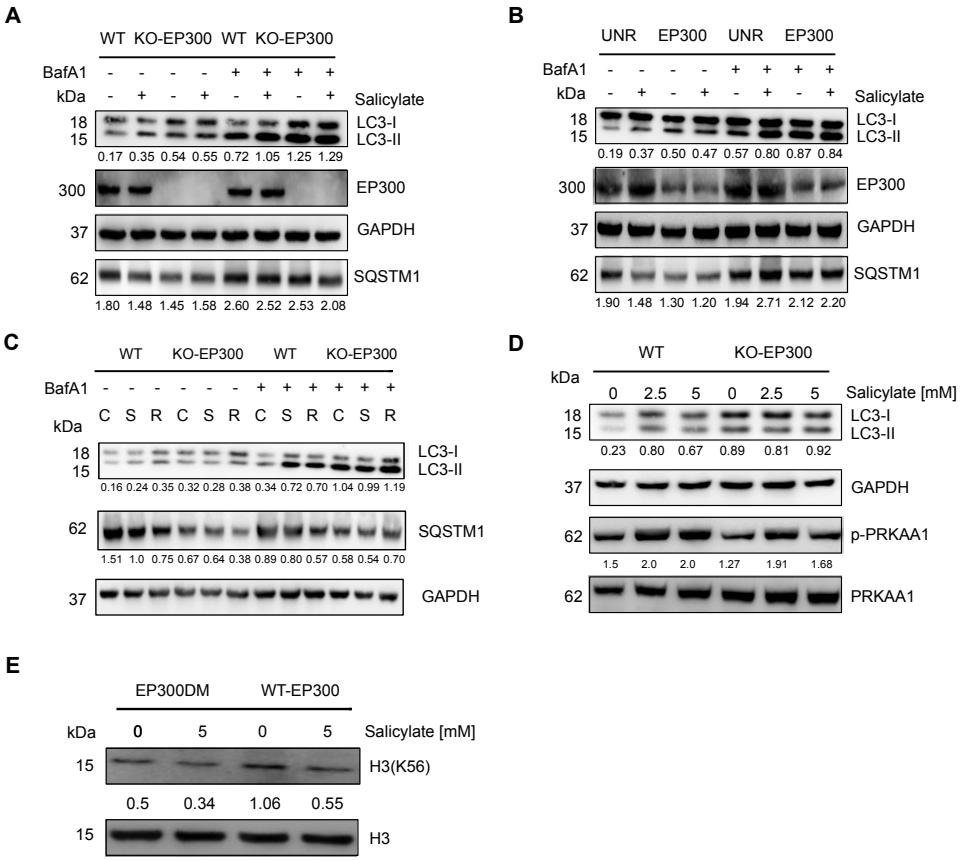

Supplemental Figure 2 (related to Figure 2 and 3) Salicylate-induced autophagy depends on EP300 inhibition (**A**) Administration of salicylate (5 mM) to HCT116 cells induces autophagy in wild type (WT) yet fails to further up regulate autophagy in KO-EP300 cells, as measured by LC3-I to LC3-II conversion and SQSTM1 degradation in presence or absence of BafA1 (one representative experiment, n=3) (**B**) Representative immunoblots of U2OS cells transfected with siRNA sequences specifically targeting EP300. Salicylate triggers autophagy in unrelated siRNA condition yet does not further increase autophagy upon EP300 depletion. (**C**) mTORC1 inhibition by Rapamycin induces autophagy in KO-EP300 cells. EP300 WT cells and their KO-EP300 counterpart were treated with salicylate (S) and rapamycin (R) and autophagy was monitored in these settings. (n=2) (**D**) Ablation of EP300 does not affect salicylate-induced activation of PRKAA1. Representative immunoblots (n=2) depicting LC3I to LC3-II conversion and PRKAA phosphorylation upon treatment with growing doses of salicylate (**E**) Mutated form of EP300 reduces salicylate binding yet does not impair EP300-acetyltransferase activity. EP300-KO cells were transfected with WT-EP300 or EP300DM plasmids. EP300 activity mas monitored through measurement of EP300 substrate H3K56 acetylation.

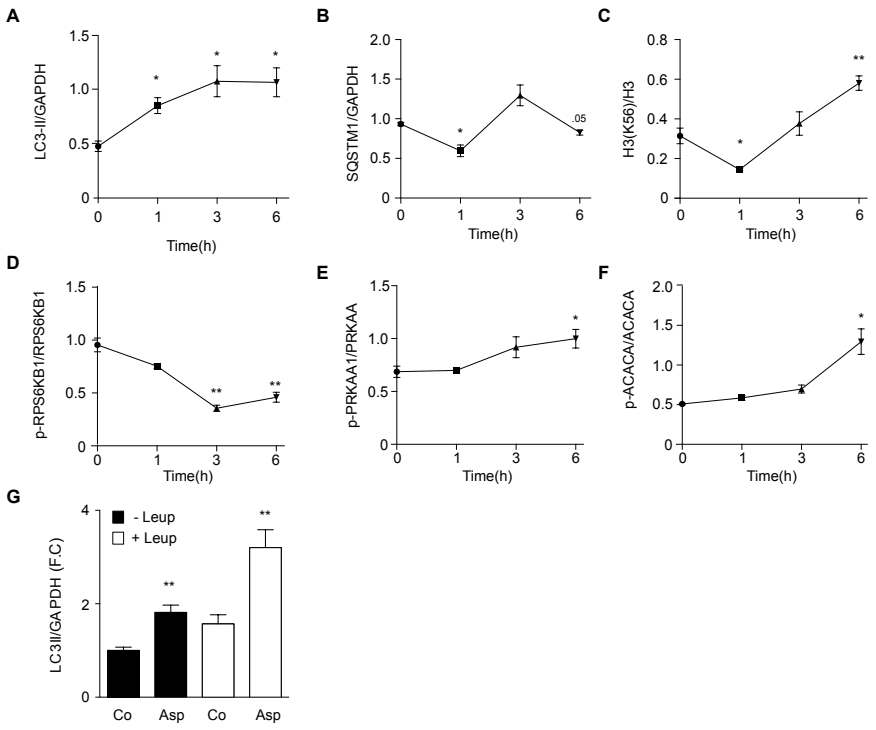

Supplemental Figure 3 (related to Figure 4). (A-F) Quantification of immunoblots depicted in **Figure 4A**, related to aspirin effect in the heart. Data represent means ± S.E.M. (Standard Error of the Mean) **p< 0.01; *p< 0.05 compared to untreated mice (unpaired *t* test). (**G**) Quantification of immunoblots depicted in **Figure 4C**, related to the measurement of autophagic flux in presence of Leupeptin in the heart. Data represent means ± S.E.M. **p< 0.01 (unpaired *t* test, compared to the respective controls).

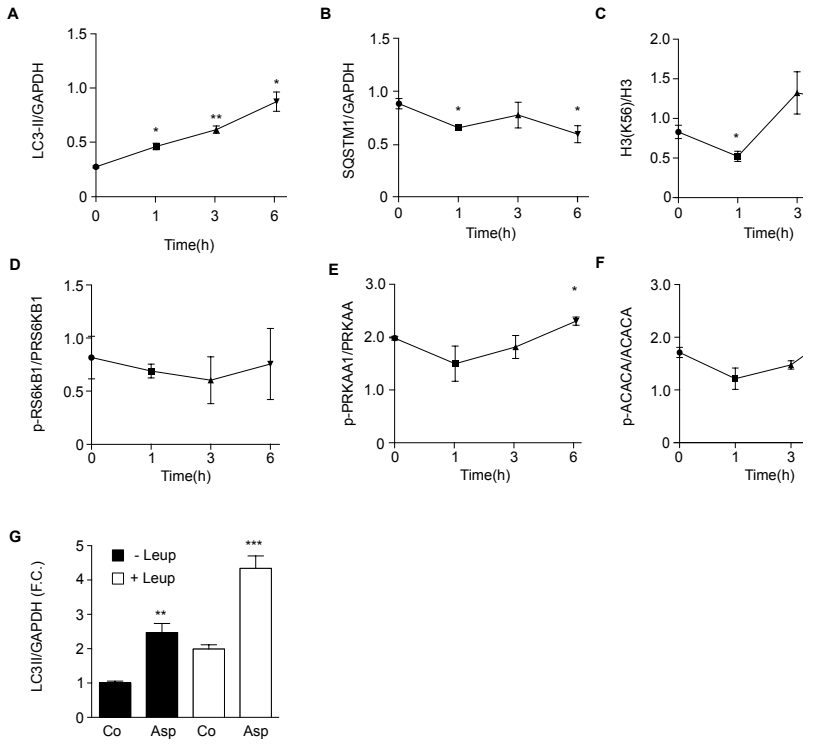

Supplemental Figure 4 (related to Figure 5). Quantification of immunoblots depicted in Figure 4B, related to aspirin effect in the liver. Data represent means means ± S.E.M. **p< 0.01; *p< 0.05 compared to untreated mice (unpaired *t* test). (**G**) Quantification of immunoblots depicted in **Figure 4D**, related to the measurement of autophagic flux in presence of Leupeptin in the liver. Data represent means ± S.E.M. *** p< 0.001; **p< 0.01; (unpaired *t* test, compared to respective controls).

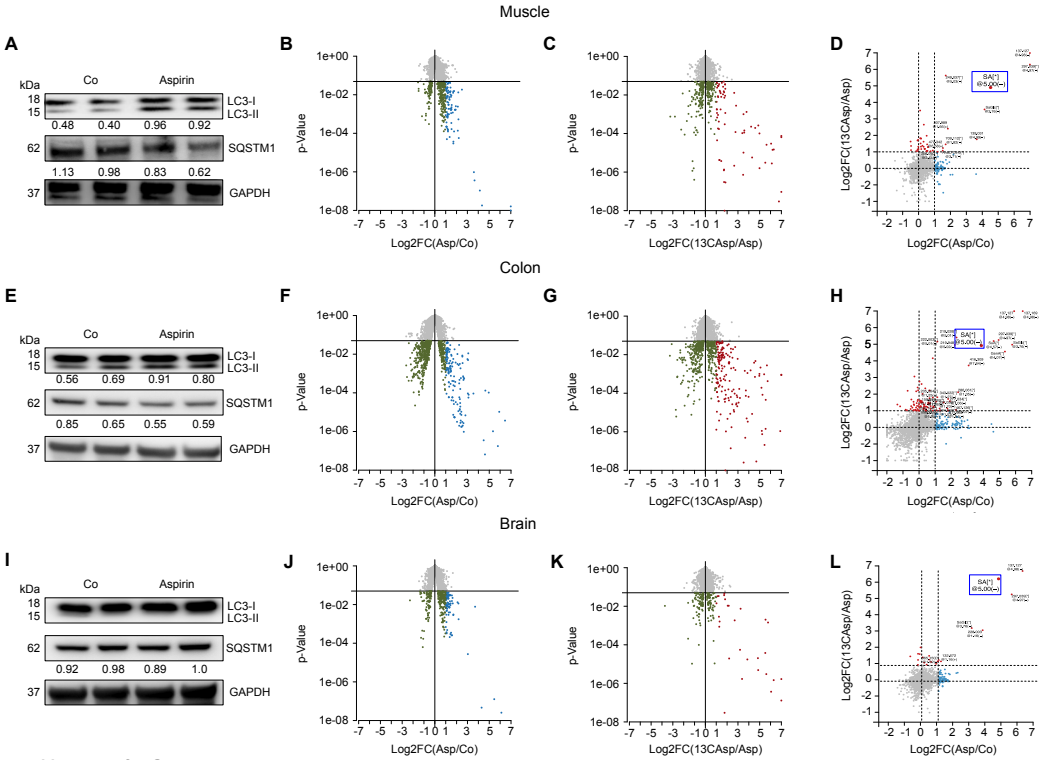

Supplemental Figure 5 (related to Figure 5). Effects of aspirin administration on autophagy and metabolomics analysis of aspirin derived metabolites in muscle, colon and brain. (**A,E,I**). Immunoblots from one representative experiment (n=2) depicting LC3-I to LC3-II conversion and SQSTM1 degradation in the indicated organs one hour after aspirin administration. Aspirin administration triggers autophagy in mice gastrocnemius muscle (**A**) and colon (**E**) yet fails to stimulate autophagy in the brain (**I**). GAPDH was used to monitor equal protein loading among lanes. (**B,F,J**). Volcano plots related to muscle (**B**), colon (**F**) and brain (**J**) of mice injected with unlabeled Aspirin as detected by mass spectrometry coupled with liquid chromatography (LC-MS) are shown. Log2FC of Asp/Co down regulated (green) or up regulated (blue) metabolites < 0.05 is represented. (**C,G,K**) Log2FC of ^{13}CAsp/Asp down regulated (green) or up regulated (red) metabolites with p value < 0.05 in muscle (**C**), colon (**G**) and brain (**K**) as detected by LC-MS after [^{13}C]-Aspirin injection to mice. (**D,H,L**) Log2FC comparison between ^{13}CAsp/Asp (red) and Asp/Co (blue) significantly changed metabolites (p value < 0.05) in muscle (**D**), colon (**H**) and brain (**L**) is depicted. Blue boxes highlight salicylate, which represents a commonly upregulated metabolite in all the organs assessed.

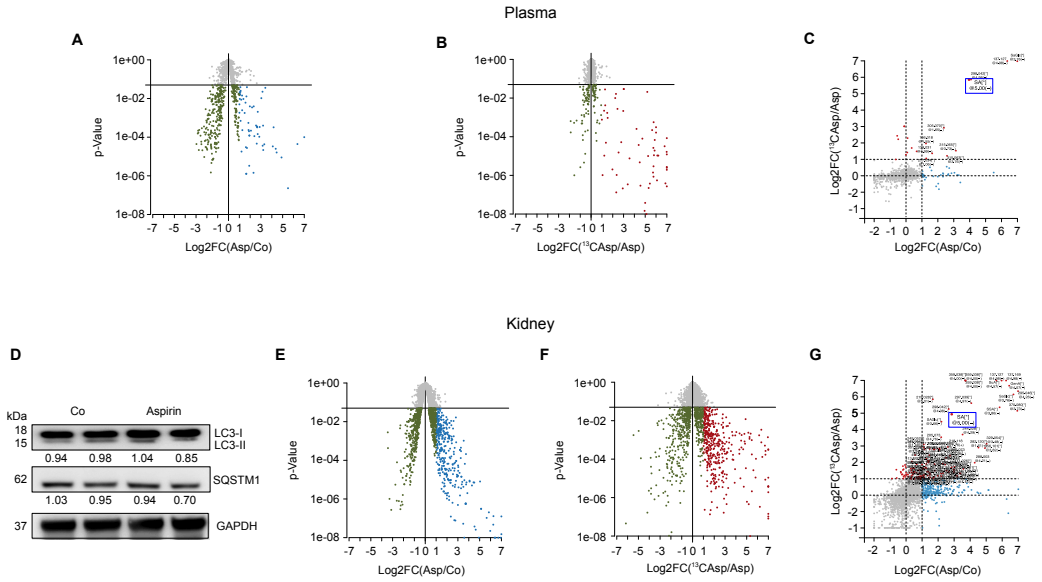

Supplemental Figure 6 (related to Figure 6). Effects of aspirin administration on autophagy and metabolomics analysis of aspirin derived metabolites in mice plasma and kidney. (**A,E**) Volcano plots related to plasma (**A**) and kidney (**E**) of mice injected with unlabeled Aspirin as detected by LC-MS are shown. Log2FC of Asp/Co down regulated (green) or up regulated (blue) with p value < 0.05 is represented. (**B,F**) Log2FC of ^{13}CAsp/Asp down regulated (green) or up regulated (red) metabolites with p value < 0.05 in plasma (**B**) and kidney (**F**) as detected by LC-MS after [^{13}C]-Aspirin injection to mice. (**C,G**) Log2FC comparison between ^{13}CAsp/Asp (red) and Asp/Co (blue) (blue) significantly changed metabolites (p value < 0.05) in plasma (**C**) and kidney (**G**) is depicted. Blue boxes highlight salicylate, which represents a commonly upregulated metabolite in all the organs assessed. (**D**) Immunoblots from one representative experiment (n=2) showing LC3-I to LC3-II conversion and SQSTM1 degradation in the kidney of mice one hour after aspirin injection.

Experimental Procedures

Docking computational modeling. In order to test the working hypothesis that Aspirin (and its metabolite salicylate) prevents the binding of Acetyl Coenzyme A to the active site of CBP/EP300, docking of salicylate to EP300 (Protein Database Structure: 3BIY) was analysed by means of Glide extra-precision (Glide XP) software based on the previously described interaction between Lys-CoA and EP300/CBP. (Liu et al., 2008) Docking predicts that the salicylate molecule engages in several interactions with the enzyme, among those some key hydrophobic as well as key polar interactions. Of particular interest are the hydrophobic interactions between Tyr1414 (end-on pi-stacking between CG1-H of Tyr1414 and the pi-cloud of the aromatic ring of salicylate) and salicylate, as well as

between Trp1466 (end-on pi-stacking between C3-H [adjacent to carboxylic acid function] and the pi-cloud of the aromatic 5-ring of Trp1466). In the complex crystal structure of p300/CBP and Lys-CoA (Protein Database Code: 3BIY) Tyr1414 is not involved in particular interactions with the bi-substrate inhibitor, and Trp1466 engages (through its side-chain NH) in a hydrogen bond with the inhibitor. Taking into account the differences in interactions made by Tyr1414 and Trp1466, the following mutations are proposed:

1) Mutation of Tyr1414 into Ala. This mutation should abolish the possibility of hydrophobic or pi-stacking interactions with the salicylate, without having a negative impact on Acetyl-CoA binding
2) Mutation of Trp1466 into Lys. This mutation should abolish the possibility of pi-stacking interactions with the salicylate, while maintaining a polar (hydrogen bonding) interaction with the phosphate of Lys-CoA.

Metabolomics experiment

Sample preparation Tissue

6-weeks old C57BL/6 mice were injected with unlabeled Aspirin or with Acetylsalicylic-α-[^{13}C] on 99 atom (#603287, Sigma Aldrich) and euthanized 1 h later. About 30mg of tissues for each condition were first weighted and solubilized into 1.5 mL polypropylene microcentrifuge tubes, with 1 ml of cold lysate buffer (MeOH/Water/Chloroform, 9/1/1, -20°C). They were then homogenized three times for 20 s at 5500 rpm using Precellys 24 tissue homogenator (Bertin Technologies), followed by centrifugation (10min at 15000g, 4°C). Upper phase of the supernatant (600µl) was collected and evaporated in microcentrifuge tubes at 40°C in a pneumatically-assisted concentrator (Techne DB3). On dried extract, 300µl of methanol was added. Upper fraction of 150µl was collected and evaporated. The dried extract was solubilized with 300µl of MilliQ water, centrifugate (10min at 15000g 4°C) and aliquoted in 3 microcentrifuge tubes (100µl). Aliquots were transferred in UHPLC vials and injected into UHPLC/MS or kept at -80 °C until injection.

Sample preparation plasma (lithium heparin)

A volume of 50µl of plasma was mixed with a cold solvent mixture (MeOH/Water/Chloroform, 9/1/1, -20°C), into 1.5 mL polypropylene microcentrifuge tubes, vortexed and centrifugated (10min at 15000g, 4°C). On dried extract, 300µl of methanol was added. Upper fraction of 150µl was collected and evaporated. The dried extract was solubilized with 300µl of MilliQ water, centrifugate (10min at 15000g 4°C) and aliquoted in 3 microcentrifuge tubes (100µl). Aliquots were transferred in UHPLC vials and injected into UHPLC/MS or kept at -80 °C until injection.

Untargeted analysis of intracellular metabolites by ultra-high performance liquid chromatography (UHPLC) coupled to a quadrupole-time of flight (QTOF) mass spectrometer.

Profiling of intracellular metabolites was performed on a Liquid Chromatography (LC) 1260 system (Agilent Technologies) coupled to a QTOF 6520 (Agilent Technologies) equipped with an electrospray source operating in both positive and negative mode and full scan mode from 50 to 1000 Da. The gas temperature was set to 350°C with a gas flow of 12 l/min. The capillary voltage was set to 3.5 kV, and the fragmentor at 120 V. Two reference masses were used to maintain the mass accuracy during analysis: m/z 121.050873 and m/z 922.009798 in positive mode and m/z 112.985587 and m/z 980.016375 in negative mode.

10 µL of sample were injected on a SB-Aq column (100 mm × 2.1 mm particle size 1.8 µm) from Agilent Technologies, protected by a guard column XDB-C18 (5 mm × 2.1 mm particle size 1.8µm) and heated at 40°C.

The gradient mobile phase consisted of water with 0.2% of acetic acid (A) and acetonitrile (B). The flow rate was set to 0.3mL/min. Initial condition is 98% phase A and 2% phase B. Molecules were then eluted using a gradient from 2% to 95% phase B in 7min. The column was washed using 95% mobile phase B for 3 minutes and equilibrated using 2% mobile phase B for 3min.

The autosampler was kept at 4°C.

Data extraction

Profiles generated by LC-QTOF were processed using an in-house set of tools that convert raw MS data into a matrix compatible with statistical analysis. Raw data files were treated with the Molecular Feature Extraction (MFE) algorithm of the MassHunter Quantitative Analysis software, in order to identify predominant ions in form of triplets [mass to charge ratio (m/z); retention time (RT); intensity]. Ions (1) that were flagged as isotopes by the MFE algorithm, (2) that had a mass defect

between 0.75 and 0.95, (3) with a signal intensity below 3,500, and (4) outside the 0.8–10 min RT range were discarded. Those ions where further grouped and formed the basis to derived extract ion chromatograms (EICs) across all samples (tolerance: mass=16ppm, retention time=0.5 min) to ensure that peaks missed by the vendor MFE software and their isotopes with up to two 13C (tolerance: mass=20ppm) are entering peak deconvolution and integration. The final data tables are made with the characteristics (peak area, height, m/z, retention time) of the "potentially isotopically pure" precursors (labelled as M0) and those of their 2 potential isotopomers (labelled as M1/M2 at m/z+1.0033/2.0067 from M0). For each organ or biofluid, groups of M0/M1/M2 were excluded from downstream statistical analysis if they did not meet quality control (QC) criteria calculated from (1) the pooled QC samples and (2) samples from the control or unlabelled aspirin treated animals on the M0 feature.

Statistical analysis

All statistical analyses and data representations were performed on pre-processed log2-transformed peak area. For differential analysis, moderated statistics (Ref I) were used and performed on the log2 (M0) features when comparing the effect of aspirin to the control samples (Asp/Co in the text) and on the log2(M1/M0) data matrices when comparing 13C labeled aspirin to its commercial/naturally labelled counterpart (^{13}C Asp /Asp in the text). For the latter, a large positive fold change (Log2FC in the text) demonstrates enrichment at +1.0033 m/z likely due to the 13C on the aspirin scaffold. Fold changes are reported without back-transformation alongside the associated p value. These are used to depict the heatmap on Figure 5G,H, the volcano plots and explicitly given in the **Table S2**.

C. elegans experiments.

Strains and genetics. We followed standard procedures for *C. elegans* strain maintenance (Brenner, 1974). Nematode rearing temperature was kept at 20°C. The following strains were used in this study: N2: wild-type Bristol isolate, DA2123: (*adIs2122*[p$_{lgg-1}$GFP::LGG-1 *rol-6(df)*], VK1093 (p$_{nhx-2}$*mCherry::lgg-1*), HZ589 (*him-5(e1490) V; bpIs151 [sqst-1p::sqst-1::GFP + unc-76(+)*].

Plasmid construct and RNAi. For *cbp-1* RNAi experiment, we constructed a plasmid that directs the synthesis of a dsRNA corresponding to the *cbp-1* gene in *E. coli* bacteria, which were then fed to animals according to previously described methodology (Kamath et al., 2001).To construct the *cbp-1 RNAi* plasmid, a *cbp-1* gene-specific fragment was obtained by PCR amplification directly from *C.*

elegans genomic DNA using an appropriate pair of primers (5'-CTTGCCACCACCAGATATGC-3' and 5'-ATGAACCAGTGAAGCGATGC-3'). The PCR-generated fragment was subcloned into pCRII-TOPO vector (Invitrogen) from which it was excised as a *Pst*I/*Kpn*I fragment and inserted into the corresponding sites of the pL4440 plasmid vector. Engineering of the *bec-1*, *atg-7* and *dct-1* RNAi constructs was previously described. (Tasdemir et al., 2008), (Samara et al., 2008), (Palikaras et al., 2015) All the RNAi constructs were transformed into HT115(DE3) *E. coli* bacteria, deficient for RNase III (Kamath et al., 2001).

Autophagy assessment. Synchronous populations of GFP::LGG-1 expressing animals (Kang et al., 2007) were generated by hypochlorite treatment of gravid adults to obtain tightly synchronized embryos that were allowed to develop through the L4 larval stage on OP50 seeded plates. Animals were then transferred to plates containing aspirin or sodium salicylate (at the indicated concentrations) or equal volume of ethanol. Two- day old adults were treated for ~ 5 min with a sodium hypochlorite solution. Freed embryos were collected and observed under a Zeiss Axio Imager Z2 Plus epifluorescence microscope equipped with a X40 objective lens (both from Carl Zeiss). To monitor autophagic activity in adults, nematodes expressing the SQST-1/p62::GFP and mCherry::LGG-1 transgenes were monitored on day 1 and day 2 of adulthood, as indicated. Worms were anaesthetized in 10mM sodium azide and observed using a Zeiss Axio Imager Z2 Plus Epifluorescence microscope. The number of GFP puncta in the pharyngeal region (SQST-1/p62::GFP) and mCherry puncta (mCherry::LGG-1) in the intestine were analyzed on grayscale images with a pixel depth of 8 bit (256 shades of grey) using the ImageJ software. To quantify GFP::LGG-1 upon knockdown of *cbp-1* or *dct-1*, 2-day-old adults were monitored using a Zeiss LSM 710 confocal microscope. Images were acquired with a X63 objective lens. For each animal, GFP puncta in the epidermis were counted in at least three separate regions of 208 μm^2 using *analyze particles* in ImageJ. Unless otherwise specified, all comparisons were performed using one-way ANOVA and unpaired *t*- test. For all microscopy experiments, more than 15 worms were scored in each experiment and all experiments were repeated at least twice.

Bafilomycin treatment was performed following the protocol of Pivtoraiko *et al.* (Pivtoraiko et al., 2010) with slight modifications. Wild-type animals expressing the GFP::LGG-1 reporter were transferred at the L4 molt to RNAi plates supplemented or not with aspirin (1mM) in the presence or absence of 100μg/ml bafilomycin A1 (LC Laboratories). Next day, young adults were allowed to lay

eggs for a limited time interval (4-5h), and then removed. Embryos were allowed to develop into L3 molt stage and then harvested for documentation as previously described.

Mitophagy measurements. Transgenic animals expressing mitochondria-targeted Rosella (mtRosella) biosensor in body wall muscle cells (Palikaras et al, 2015) were allowed to lay eggs on plates containing 1mM aspirin or equal volume of vehicle. Vehicle- and aspirin-treated animals were harvested at 3 day of adulthood and images were acquired using a X10 objective lens.

GFP-LC3 Immunoprecipitation. 5 x 10^6 HCT116 cells stably expressing a GFP-LC3 transgene were incubated for 16 hours with 5 mM sodium salicylate and for 6 hours with nutrient free medium respectively. At the end of the treatment cells were harvested and lysed in RIPA buffer and GFP-LC3 fusion protein was immunoprecipitated by means of GFP-Trap A system (#gt-250, Chromotek) as described by manufacturer. Total lysates and GFP immunoprecipitated was probed with an antibody recognizing GFP (to assess immunoprecipitation of GFP-LC3 tandem protein) and with an antibody specifically recognizing N-Acetylated protein residues. Levels of LC3 acetylation were normalized on GFP-immunoprecipitated signal.

Long-lived proteins degradation assay. HCT116 cells were incubated for 18 h at 37 °C with 0.2 μCi/mL-[14C] valine. Unincorporated radioisotope was removed by three rinses with phosphate-buffered saline (pH 7.4). Cells were then incubated in nutrient- and serum-free medium (without amino acids and in the absence of fetal calf serum) plus 0.1% bovine serum albumin and 10 mM unlabeled valine. When required, 10 mM 3-methyladenine (#M9281, Sigma Aldrich), a potent inhibitor of the formation of autophagic vacuoles, or 4 × AA were added throughout the chase period. After the first hour of incubation, at which time short-lived proteins were being degraded, the medium was replaced with the appropriate fresh medium (in presence or absence of 5 mM sodium salicylate) and the incubation was continued for an additional 16 h period. Cells and radiolabeled proteins from the 16 h chase medium were precipitated in 10% (v/v) trichloroacetic acid at 4 °C. The precipitated proteins were separated from soluble radioactivity by centrifugation at 600 × g for 10 min and then dissolved in 250 μl Soluene 350. The rate of protein degradation was calculated as acid-soluble radioactivity recovered from both cells and the medium.

Plasmids mutagenesis and transfection. Mutations in EP300 WT sequence were introduced by means of site-directed mutagenesis (#E0054, Q5® Site-Directed Mutagenesis Kit, New England Biolabs) using specifically designed primers. Transfection of EP300 WT plasmid and its mutated counterparts was performed using Fugene Transfection Reagent (#E2311, Promega).

Automated microscopy. Human U2OS osteosarcoma and HCT116 colorectal cancer cells stably expressing GFP-LC3 were seeded in 96-well or 384-wells imaging plates (BD Falcon, Sparks, USA) twenty-four h before stimulation to reach 70% confluence. Cells were treated with the indicated agents in absence or presence of the lysosomal inhibitor BafA1 (for the last two h of treatment) Subsequently, cells were fixed with 4% PFA and counterstained with 10 μM Hoechst 33342. Images were acquired using a BD pathway 855 automated microscope (BD Imaging Systems, San Jose, USA) equipped with a 40X objective (Olympus, Center Valley, USA) coupled to a robotized Twister II plate handler (Caliper Life Sciences, Hopkinton, USA). Images (5x5 frames), corresponding to 100-500 cells/well, were analyzed for the detection of GFP-LC3 puncta in the cytoplasm by means of the BD Attovision software (BD Imaging Systems). Cellular regions of interest, cytoplasm and nucleus, were defined and segmented according to standard procedures. RB 2x2 and Marr-Hildreth algorithms were employed to allow the detection of GFP LC3 puncta. Statistical analyses were conducted using Prism software.

Chemicals and culture conditions. Unless otherwise indicated, media and supplements for cell culture were purchased from Gibco-Thermo Fisher Scientific while plastic ware was purchased from Corning B.V. Life Sciences. Human osteosarcoma U2OS and their green fluorescent protein (GFP)-LC3-expressing derivatives (gift from Professor J. Yuan, Harvard University), were cultured in DMEM medium (#11965-092, Thermo Fisher Scientific) supplemented with 10% (v/v) fetal bovine serum (#10082139, Thermo Fisher Scientific), 100 mg/L sodium pyruvate (#11360070, Thermo Fisher Scientific) 10 mM HEPES buffer (#15630080, Thermo Fisher Scientific), 100 IU mL^{-1} penicillin G sodium salt, and 100 mg/mL streptomycin sulfate (#15140122, Thermo Fisher Scientific). Human colorectal cancer HCT116 wild type or EP300 knockout (purchased from Cancer Technology, upon MTA:008927) and their GFP-LC3-expressing derivatives were cultured in McCoy medium (#16600-082, Thermo Fisher Scientific) supplemented with 10% (v/v) fetal bovine serum, 100 mg/L sodium pyruvate, 10 mM HEPES buffer, 100 IU mL^{-1} penicillin G sodium salt, and 100 mg/mL streptomycin sulfate. Murine embryonic fibroblast (MEF) wild type cells and PRKAA $\alpha1/\alpha2^{-/-}$ (gift from Dr. B.

Viollet, Cochin Institut) were cultured in DMEM medium supplemented with 10% (v/v) fetal bovine serum, 100 mg/L sodium pyruvate, 10 mM HEPES buffer, 100 IU mL^{-1} penicillin G sodium salt, and 100 mg/mL streptomycin sulfate and 1 mM non-essential amino acids. All cells were maintained in standard culture conditions (at 37 ºC, under 5% CO2). Cells were seeded in 6-well, 96-wells or 384 well plates before treatment with 1.25 to 5 mM acetylsalicylic acid (#A5376, Sigma Aldrich) and sodium salicylate (#S3007, Sigma Aldrich), 10 μM C646 (#SML0002, Sigma Aldrich), 50 μM anacardic Acid (#A7236, Sigma Aldrich), 1.25 to 5 mM Ethyl-Salicylate (#112291, Sigma Aldrich), 100 nM bafilomycin A1 (#B1080, LC Laboratories), 1 μM Rapamycin (#R-5000, LC Laboratories).

Immunoblotting. For immunoblotting, protein extracts obtained by cellular lysis in radioimmunoprecipitation assay buffer (RIPA) buffer were run on 4-12% Bis-Tris acrylamide gels (#NP0322, Thermo Fisher Scientific) and electrotransferred to 0.2 μM polyvinylidene fluoride (PVDF) membranes (#1620177,Bio-Rad). Non-specific binding sites were saturated by incubating membranes for 1 h in 0.05% Tween 20 (#P9416, Sigma Aldrich) v:v in Tris-buffered saline (TBS) (#ET220, Euromedex) supplemented with 5% non-fat powdered milk (w:v in TBS), followed by an overnight incubation with primary antibodies specific for LC3B (#2775 Cell Signaling Technology), phospho-PRKAAα (Thr172) (#2531, Cell Signaling Technology), PRKAAα (#2532, Cell Signaling Technology), phospho-ACC (Ser79) (#3661, Cell Signaling Technology), ACC (#3662, Cell Signaling Technology), phospho-ribosomal protein S6 kinase (Thr389)(#9205, Cell Signaling Technology), ribosomal protein S6 kinase (#9202, Cell Signaling Technology), EP300 (N-15) (#sc-584,Santa-Cruz Biotechnology), SQSTM1/p62 (#H00008878-M0, Abnova), H3 (Lys56) (#4243, Cell Signaling Technology), H3 (#9715, Cell Signaling Technology), H2A (Lys5) (#2576, Cell Signaling Technology), H2A (#2578, Cell Signaling Technology), GFP (#2956, Cell Signaling Technology), Acetylated Lysine antibody (#9441, Cell Signaling). Membranes were cut in order to allow simultaneous detection of different molecular weight proteins. Equal protein loading was monitored by probing membranes with a glyceraldeyde-3-phosphate dehydrogenase (GAPDH)-specific antibody (#2118, Cell Signaling Technology). Membranes were developed with suitable horseradish peroxidase conjugates followed by chemiluminescence-based detection with the Amersham ECL Prime (#RPN2232, GE Healthcare and the ImageQuant LAS 4000 software-assisted imager (GE Healthcare, Piscataway, NJ, USA). Quantification was performed by densitometry by means of Image J software.

Autophagy was quantified through evaluation of LC3-II/GAPDH ratio and SQSTM1/GAPDH ratio according to (Klionsky et al., 2016). Posttranslational modifications (phosphorylation and acetylation) of specific residues were normalized on the levels of the respective total protein after membrane stripping (#21059, Thermo Fisher Scientific).

RNA interference in cell culture. Two different small interfering RNA (siRNA) sequences targeting EP300 (#6224, #6237; Sigma Aldrich) and PRKAA (#EHU074041 and #HA02727114, Sigma Aldrich) were reversed transfected by means of Lipofectamine RNAi MAX (#13778030, Thermo Fisher Scientific) transfection reagent.

Mouse experiments and tissue processing. For short-term autophagy induction studies, mice were treated with 100 mg/kg *i.p*. acetylsalicylic acid (Asp) 1 to 6 h after aspirin administration. To assess autophagic flux, 30 mg/kg *i.p.* leupeptin (SP-04-2217-A, Euromedex**)** was injected 2 hours before sacrifice. After treatment mice were euthanized and tissues were snap-frozen in liquid nitrogen after extraction and homogenized two cycles for 20 s at 5.500 rpm using a Precellys 24 tissue homogenator (Bertin Technologies) in 20 mM Tris buffer (pH 7.4) containing 150 mM NaCl, 1% Triton X-100, 10 mM EDTA and Complete® protease inhibitor cocktail (#000000011873580001, Sigma Aldrich). Tissue extracts were then centrifuged at 12,000 g at 4 ºC and supernatants were collected. Protein concentration in the supernatants was evaluated by the bicinchoninic acid technique (#23225, BCA protein assay kit). For cardiac mitophagy assessment, 2 months-old mito-Keima transgenic mice were treated for 2 weeks by oral gavage (five times a week) with aspirin (25 mg/kg), suspended in water. Fresh tissues were used for confocal microscopy studies. Heart tissues were rapidly taken out and rinsed with cold PBS. Thereafter, they were cut by a vibrating microtome within cold PBS into 10-15 sections (each 250μm). These sections were placed into a refrigerator (4°C) and immediately analyzed. Fluorescent samples were examined with a confocal microscope (Nikon Eclipse Ti). The excitation spectrum of the fluorescent probe mito-Keima varies according pH. While a short wavelength (457 nm) predominates at neutral pH, a longer (561 nm) wavelength prevails at low pH environment (corresponding to recruitment of mitochondria to lysosomes). Conditions of up regulated mitophagy are thus characterized by an elevated 561/457 ratio (quantified as mitophagy area).

For the evaluation of autophagic flux, 2-month-old Tg-tf-LC3 mice were treated for 2 weeks by oral gavage (five times a week) with aspirin (25 mg/kg), suspended in water. Chloroquine (#C6628, Sigma Aldrich) (10 mg/kg) was injected intraperitoneally 4 h before euthanasia. For in vivo determination of the number of fluorescent LC3 dots, fresh heart slices were embedded with tissue-TEK OCT compound (Sakura Fine technical Co., Ltd.) and frozen at -80 °C. 10-μm-thick sections were obtained from the frozen tissue samples by using a cryostat (CM3050S; Leica), air-dried for 30 min, fixed by 10% formalin for 10 min, mounted by using a reagent containing DAPI, and viewed under a fluorescence microscope.

Supplemental References

Brenner, S. (1974). The genetics of Caenorhabditis elegans. Genetics *77*, 71-94.

Kamath, R.S., Martinez-Campos, M., Zipperlen, P., Fraser, A.G., and Ahringer, J. (2001). Effectiveness of specific RNA-mediated interference through ingested double-stranded RNA in Caenorhabditis elegans. Genome Biol *2*, RESEARCH0002.

Kang, C., You, Y.J., and Avery, L. (2007). Dual roles of autophagy in the survival of Caenorhabditis elegans during starvation. Genes Dev *21*, 2161-2171.

Liu, X., Wang, L., Zhao, K., Thompson, P.R., Hwang, Y., Marmorstein, R., and Cole, P.A. (2008). The structural basis of protein acetylation by the p300/CBP transcriptional coactivator. Nature *451*, 846-850.

Palikaras, K., Lionaki, E., and Tavernarakis, N. (2015). Coordination of mitophagy and mitochondrial biogenesis during ageing in C. elegans. Nature *521*, 525-528.

Pivtoraiko, V.N., Harrington, A.J., Mader, B.J., Luker, A.M., Caldwell, G.A., Caldwell, K.A., Roth, K.A., and Shacka, J.J. (2010). Low-dose bafilomycin attenuates neuronal cell death associated with autophagy-lysosome pathway dysfunction. J Neurochem *114*, 1193-1204.

Samara, C., Syntichaki, P., and Tavernarakis, N. (2008). Autophagy is required for necrotic cell death in Caenorhabditis elegans. Cell Death Differ *15*, 105-112.

Tasdemir, E., Chiara Maiuri, M., Morselli, E., Criollo, A., D'Amelio, M., Djavaheri-Mergny, M., Cecconi, F., Tavernarakis, N., and Kroemer, G. (2008). A dual role of p53 in the control of autophagy. Autophagy *4*, 810-814.